Coordinated Control of SMES and DVR for Improving Fault Ride-Through Capability of DFIG-based Wind Turbine

Fatma BOUAZIZ [*], Abdelkarim MASMOUDI [*], Achraf ABDELKAFI [*‡], Lotfi KRICHEN [*]

[*] University of Sfax, National Engineering School of Sfax, Electrical Systems and Renewable Energies Laboratory (LSEER), BP 1173, Sfax 3038, Tunisia

(fatma.bouaziz@enis.tn, abdelkarim.masmoudi@enetcom.usf.tn, achraf.abdelkafi@enis.tn, lotfi.krichen@enis.tn)

‡Corresponding Author; Achraf ABDELKAFI, National Engineering School of Sfax, Electrical Systems and Renewable Energies Laboratory (LSEER), BP 1173, 3038, Sfax, Tunisia, Tel.: (+216) 74 274 418 / Fax: (+216) 74 275 595, achraf.abdelkafi@enis.tn

Received: 23.12.2021 Accepted: 17.01.2022

Abstract- High voltage ride through (HVRT) and low voltage ride through (LVRT) may result in serious problems when doubly fed induction generator-based wind turbine (DFIG_WT) is connected to the electrical grid. This paper investigates on the integration of a dynamic voltage restorer (DVR) and a superconducting magnetic energy storage system (SMES) with the conventional structure. This novel configuration enhances the fault ride-through (FRT) capability of the DFIG_WT in order to maintain production even in case of grid defects. The SMES was coupled in parallel to the dc-link in order to regulate the capacitor voltage through the DC/DC chopper and to ensure the energy exchange with the grid in both directions. The DVR is used to compensate the voltage unbalance on the system terminals. Simulation results of different applied fault were presented in order to prove the robustness of the proposed control strategies and to validate the performance found by the integration of the DVR _SMES with the DFIG_WT.

Keywords Doubly fed induction generator, fault ride-through, superconducting magnetic energy storage, dynamic voltage restorer.

Nomenclature

V_w	wind speed, $(m\ s^{-1})$	$I_{sd,q}$	$d-q$ components of the stator currents, (A)
ρ	air density, $(1.22\ Kg\ m^{-3})$	$I_{rd,q}$	$d-q$ components of the rotor currents, (A)
R	blade radius, (m)	$\phi_{sd,q}$	stator $d-q$ frame flux, (Wb)
C_p	power coefficient	$\phi_{rd,q}$	rotor $d-q$ frame flux, (Wb)
λ	tip speed ratio	R_f	filter resistance, (Ω)
β	pitch angle, $(°)$	L_f	filter inductance, (H)
Ω_t	rotor speed of the wind turbine, $(rad\ s^{-1})$	$V_{fd,q}$	$d-q$ components of the filter voltages, (V)
Ω_m	rotor speed of the DFIG, $(rad\ s^{-1})$	$I_{fd,q}$	$d-q$ components of the filter currents, (A)
P_{aer}	aerodynamic power, (W)	$V_{Gd,q}$	$d-q$ components of the grid voltages, (V)
T_{aer}	aerodynamic torque, (Nm)	I_g	grid current, (A)
T_{em}	electromagnetic torque, (Nm)	C	dc-link capacitance, (μF)
T_m	mechanical torque, (Nm)	V_{dc}	dc-link voltage, (V)
f_v	coefficient of viscous friction, $(N.m.s.rad^{-1})$	L_{dvr}	filter inductance of the DVR, (H)

J	moment of inertia, $(Kg\ m^2)$	C_{dvr}	filter capacitance of the DVR, (μF)
R_{sl}	stator winding resistance, (Ω)	I_c	correction of distortion current, (A)
R_r	rotor winding resistance, (Ω)	I_{ff}	current produced by the DVR, (A)
L_{sl}	stator winding inductance, (H)	V_{ff}	filter voltage of the DVR, (V)
L_r	rotor winding inductance, (H)	L_{smes}	SMES inductance, (H)
M	mutual inductance, (H)	V_{smes}	SMES voltage, (V)
σ	leakage coefficient, $\sigma = 1\ \left(M^2/L_{sl}L_r\right)$	I_{smes}	SMES current, (A)
ω_s	stator $d-q$ reference axes speed, $\left(rad\ s^{-1}\right)$	I_{smes_0}	SMES initial current, (A)
ω_r	rotor $d-q$ reference axes speed, $\left(rad\ s^{-1}\right)$	I_{chop}	chopper current, (A)
p	number of pole pairs	P_{smes}	SMES power, (W)
$V_{sd,q}$	$d-q$ components of the stator voltages, (V)	W_{smes}	SMES energy, (J)
$V_{rd,q}$	$d-q$ components of the rotor voltages, (V)	W_{smes_0}	SMES initial energy, (J)

1. Introduction

Renewable energies have been more and more developed in recent years for the electricity production. Wind power is one of the renewable energy sources that become the most important and the most promising one in the world in terms of development [1].

The DFIG based wind turbine with variable speed technology is still the most used one, especially in the high power network integration. The DFIG has several advantages such as high energy efficiency, good robustness and the power converters are sized to only 30% of the total rated power which reduces the installation cost [2,3]. However, DFIG is very sensitive to network disturbances and particularly when the electrical network is subjected to voltage drop or swell [3]. This type of fault leads to an increase in the stator current. Because of the magnetic coupling between the stator and the rotor, the fault current will flow through the rotor and create a peak current in the winding with an increase in the DC bus voltage which can damage the power converters [4,5]. Therefore, many researches were investigated to overcome problems in DFIG _WT structure in order to improve the fault ride through capability during various types of fault. The developed techniques can be classified into two categories. The first one is a software solution which consists in modifying the control technique applied to the converters in case of faults [6-9]. However, this solution is available only for small voltage variations [10-12]. The second one is a hardware solution by adding a crowbar protection which is frequently used to limit the dc link voltage instability and the over-current in the rotor and stator windings. In Ref. [13], the use of superconducting fault current limiter (SFCL) associated in series with the rotor allows a fast limitation of the rotor current. A DC chopper is linked in parallel with the dc link to dissipate the excessive energy and to keep the dc-link voltage within the suitable range. In Ref. [14], the modified DC chopper is able to limit the over-current in the stator and allows the control of the dc link capacitor during weak voltage, but it is used with many semiconductor switches that allow inserting the resistance in shunt or in parallel with the dc link. In Ref. [15], shunt voltage compensation (SVR) and static synchronous compensator (STATCOM) improve the voltage stability by giving appropriate reactive power compensation in a short period. In Ref [16], authors proposed an AC voltage generator based on a DVR and a supercapacitor storage device with the DFIG WT in order to circumvent the grid voltage perturbation with the improvement of FRT capability. Refs. [17,18] reveal that the dynamic voltage restorer (DVR) has the ability to enhance the FRT capability of the DFIG by the injection of the desired voltage at the WT terminals . Each of the protection devices has an advantage over the other devices. Moreover, the cost and the size of the DVR are lower than the STATCOM [19]. In Ref. [20] authors investigate about the performance of using SMES with DFIG WT for improving grid power stability with two possible connections. The first one on the dc-link and the second one on the common coupling point (PCC). Authors in Ref. [21] studied the effect of integrating SMES in DFIG WT for both grid-connected and standalone mode in order to enhance the stability of the whole system in case of different faults scenarios.

Some research has combined two strategies to overcome the FRT problem. In Ref [22], authors studied the impact of using STATCOM associated with SMES in the DFIG WT structure connected to the grid in case of symmetrical voltage sag. Ref. [23] showed that the coordination between SMES and resistor series limiter (RSL) with transient voltage control (TVC) may improve the global DFIG WT performance by injecting reactive and active power into the network during a fault. Ref. [24] proposed a cooperative operation of SMES and FCL with a modified control of rotor side and grid side converter in order to suppress the transient oscillation in a short time. In Ref. [25], two technologies SFCL and SMES were combined in order to suppress the over-current in the

DFIG rotor and stator, to reduce the dc-link fluctuations and also to limit the electromagnetic torque oscillation around 33.8%.

In this general context and due to several advantages found by using SMES and DVR, the proposed idea in this study is to combine a SMES and a DVR with the DFIG_WT structure and benefit from its performances to enhance the fault ride-through capability of the DFIG under-voltage swell/sag. A novel control technique of SMES_DVR was developed in order to compensate the fault effect on the considered structure and maintain the DFIG_WT connected to the grid during LVRT/HVRT.

This paper is organized as follows: the description of the studied system was developed in Section 2. The modeling of the novel configuration of the DFIG based wind turbine associated to SMES and DVR was established in Section 3. The effect of LVRT and HVRT on the WECS and the control of the novel structure were described in section 4. In section 5, simulation results show a detailed comparison between the classical control of the DFIG_WT and the proposed control in case of different grid fault. Some conclusions are given in Section 6.

2. Description of the Studied System

The DFIG based wind turbine presented in this paper is illustrated in Fig. 1. This structure comprises a variable speed wind turbine (VSWT) driving a DFIG through a gearbox associated to a SMES and a DVR. The stator of the DFIG is directly coupled to the electric grid while the rotor is coupled via two power converters, a dc-link and an RL filter. These two converters can exchange independently the active and the reactive power in both directions. Actually, when the wind speed is higher than the synchronism speed, approximately 30% of the nominal machine power can be transmitted from the rotor to the network. The DVR is connected to the DC link through a DC/AC converter in order to compensate the terminal stator voltage and to regulate the capacitor voltage at the same time. The SMES is connected to the DC link through a DC/DC converter which ensures the voltage regulation by the exchange of the required energy with the grid.

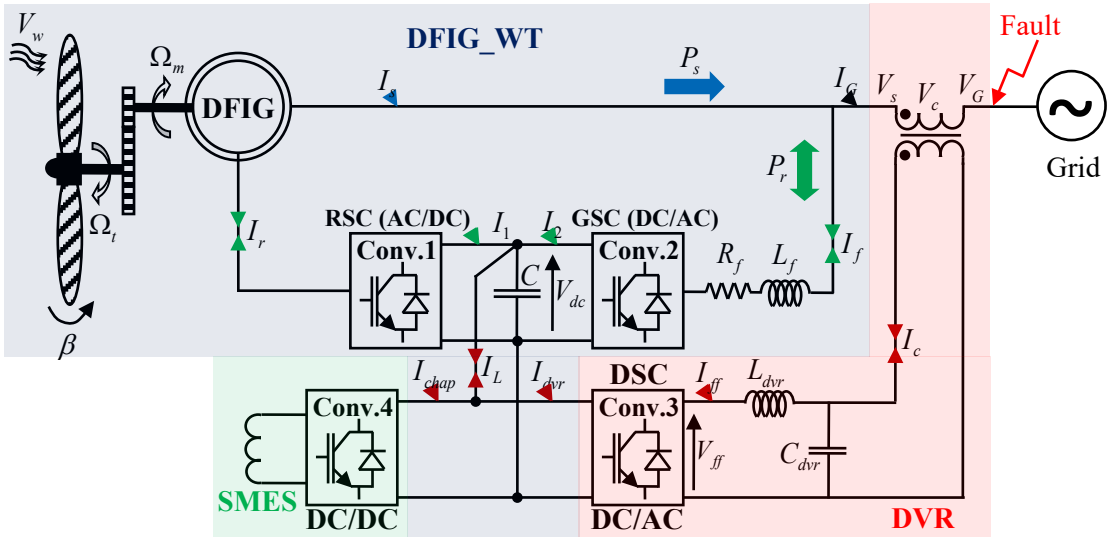

Fig. 1. Structure of DFIG_WT associated to SMES_DVR.

3. Wind Energy Conversion System Modelling

3.1. Wind turbine model

In order to investigate the WT dynamic behavior, it is necessary to simulate the mathematical model which describes the WT function [26,27].

The WT aerodynamic power can be written as follows:

$$P_{aer} = \frac{1}{2}\rho\pi R^2 V_w^2 C_p(\lambda,\beta) \tag{1}$$

In practice, the power coefficient "C_p" can never reach the theoretical value "0.593" according to the Betz law. For a 1.5 MW WT, the expression of the power coefficient is given by [28]:

$$C_p(\lambda,\beta) = (0.5 \quad 0.167(\beta \quad 2))\sin\left(\frac{\pi(\lambda+0.1)}{10-0.3\beta}\right) - 0.00184(\lambda-3)(\beta-2) \tag{2}$$

where

$$\lambda = \frac{R\Omega_t}{V_w} \tag{3}$$

From the equations of the speed turbine and the mechanical power, the equation of the aerodynamic torque is determined as follows:

$$T_{aer} = \frac{P_{aer}}{\Omega_t} \tag{4}$$

The gearbox is coupled between the WT and the generator in order to adapt the speed of the two shafts. It is expressed by the following equation:

$$G = \frac{\Omega_m}{\Omega_t} = \frac{T_{aer}}{T_m} \quad (5)$$

By applying the dynamic fundamental law, the DFIG speed can be determined by the following relation:

$$J \frac{d\Omega_m}{dt} = T_m - T_{em} - f_v \Omega_m \quad (6)$$

3.2. DFIG modelling and control

To simulate the DFIG behavior, a mathematical model in the Park reference frame is developed. The magnetic and electrical interaction between the stator and the rotor windings are written by the following equations [29,30]:

$$V_{sd} = R_{sl} I_{sd} + \frac{d\phi_{sd}}{dt} - \omega_s \phi_{sq} \quad (7)$$

$$V_{sq} = R_{sl} I_{sq} + \frac{d\phi_{sq}}{dt} + \omega_s \phi_{sd} \quad (8)$$

$$V_{rd} = R_r I_{rd} + \frac{d\phi_{rd}}{dt} - \omega_r \phi_{rq} \quad (9)$$

$$V_{rq} = R_r I_{rq} + \frac{d\phi_{rq}}{dt} + \omega_r \phi_{rd} \quad (10)$$

The magnetic flux equations of the DFIG are given by:

$$\phi_{sd} = L_{sl} I_{sd} + M I_{rd} \quad (11)$$

$$\phi_{sq} = L_{sl} I_{sq} + M I_{rq} \quad (12)$$

$$\phi_{rd} = L_r I_{rd} + M I_{sd} \quad (13)$$

$$\phi_{rq} = L_r I_{rq} + M I_{sq} \quad (14)$$

From magnetic and electric equations of the DFIG, the vector control technique gives the following relations [31]:

$$V_{rd} = \underbrace{R_r I_{rd} + \sigma L_r \frac{dI_{rd}}{dt}}_{V_{rd\,reg}} - \sigma L_r \omega_r I_{rq} - \frac{M}{L_{sl}} \frac{d\phi_{sd}}{dt} \quad (15)$$

$$V_{rq} = \underbrace{R_r I_{rq} + \sigma L_r \frac{dI_{rq}}{dt}}_{V_{rq\,reg}} + \sigma L_r \omega_r I_{rd} - \frac{M}{L_{sl}} \omega_r \phi_{sd} \quad (16)$$

Voltages "$V_{rd\,reg}$" and "$V_{rq\,reg}$" are the main quantities of the controlled system. From these voltages, the transfer function which makes relation between $\left(V_{rd\,reg}, I_{rd}\right)$ and $\left(V_{rq\,reg}, I_{rq}\right)$ is determined.

$$\frac{I_{rd}}{V_{rd\,reg}} = \frac{I_{rq}}{V_{rq\,reg}} = \frac{1}{R_r + \sigma L_r s} \quad (17)$$

Two PI controllers are used to regulate the rotor currents to the predefined references.

3.3. Power converter model

The power converter is modeled in the natural frame. The perfect commutation will be quantified by a switching function "f_{i1}" and "f_{i2}".This function can take two states; "0" in the case of an open switch and "1" in the case of a closed switch. The switches of the same cell are in complementary states:

$$f_{i1} + f_{i2} = 1 \quad ; \quad i \in \{1,2,3\} \quad (18)$$

The modulation functions "m_1" and "m_2" are given as follows:

$$\begin{pmatrix} m_1 \\ m_2 \end{pmatrix} = \begin{pmatrix} 1 & 0 & -1 \\ 0 & 1 & -1 \end{pmatrix} \begin{pmatrix} f_{11} \\ f_{12} \\ f_{13} \end{pmatrix} \quad (19)$$

3.4. Filter model

The filter "$R_f L_f$" is used to connect the rotor with the network and to reduce the harmonics produced by the power converter. The filter equations in the Park reference frame are given as follows:

$$V_{fd} = \underbrace{R_f I_{fd} + L_f \frac{dI_{fd}}{dt}}_{V_{fd\,reg}} - \omega_s L_f I_{fq} + V_{Gd} \quad (20)$$

$$V_{fq} = \underbrace{R_f I_{fq} + L_f \frac{dI_{fq}}{dt}}_{V_{fq\,reg}} + \omega_s L_f I_{fd} + V_{Gq} \quad (21)$$

Two PI controllers are used to regulate the filter currents to the predefined references.

4. Proposed Structure

The conventional structure of the DFIG_WT is very sensitive in case of grid faults and may possibly lead to a great damage in the WECS components. In order to avoid this problem and eliminate the harmful effects that could appear, the idea is to combine a SMES and a DVR with the conventional structure. The proposed control strategy depicted in Fig. 2 aims to provide stator voltage stability and regulate the dc-link capacitor in order to obtain good power quality and improve the FRT capability of the DFIG_WT.

During the fault, the DVR must inject the necessary voltage to compensate the voltage dip or swell and consequently maintain the voltage at the DFIG terminal within its admissible limits. In case of voltage dips, the DVR injects the desired voltage in phase with the "V_G" network voltage which restores the amplitude of the voltage "V_s" to their

reference. In case of an overvoltage, the DVR injects the voltage in phase opposition with the network voltage which restores the desired voltage "V_s" amplitude.

In addition to the DVR, the SMES which is capable of exchanging energy with the grid in a short time is connected to the dc-link through a buck-boost converter in order to achieve two objectives. The first one consists of regulating the dc-link voltage at an acceptable margin by exchanging the adequate DC current between the SMES coil and the capacitor. The second objective is the exchange of the desired DC current with the DSC converter in order to compensate the unbalanced grid voltage. During voltage dips, the energy is transferred from the SMES to the grid which leads to an increase of the voltage "V_G" and the voltage "V_s". In case of a voltage swell, the energy transfer will be reversed from the grid to the SMES which allows the decrease of the grid voltage and the voltage "V_s" at the same time.

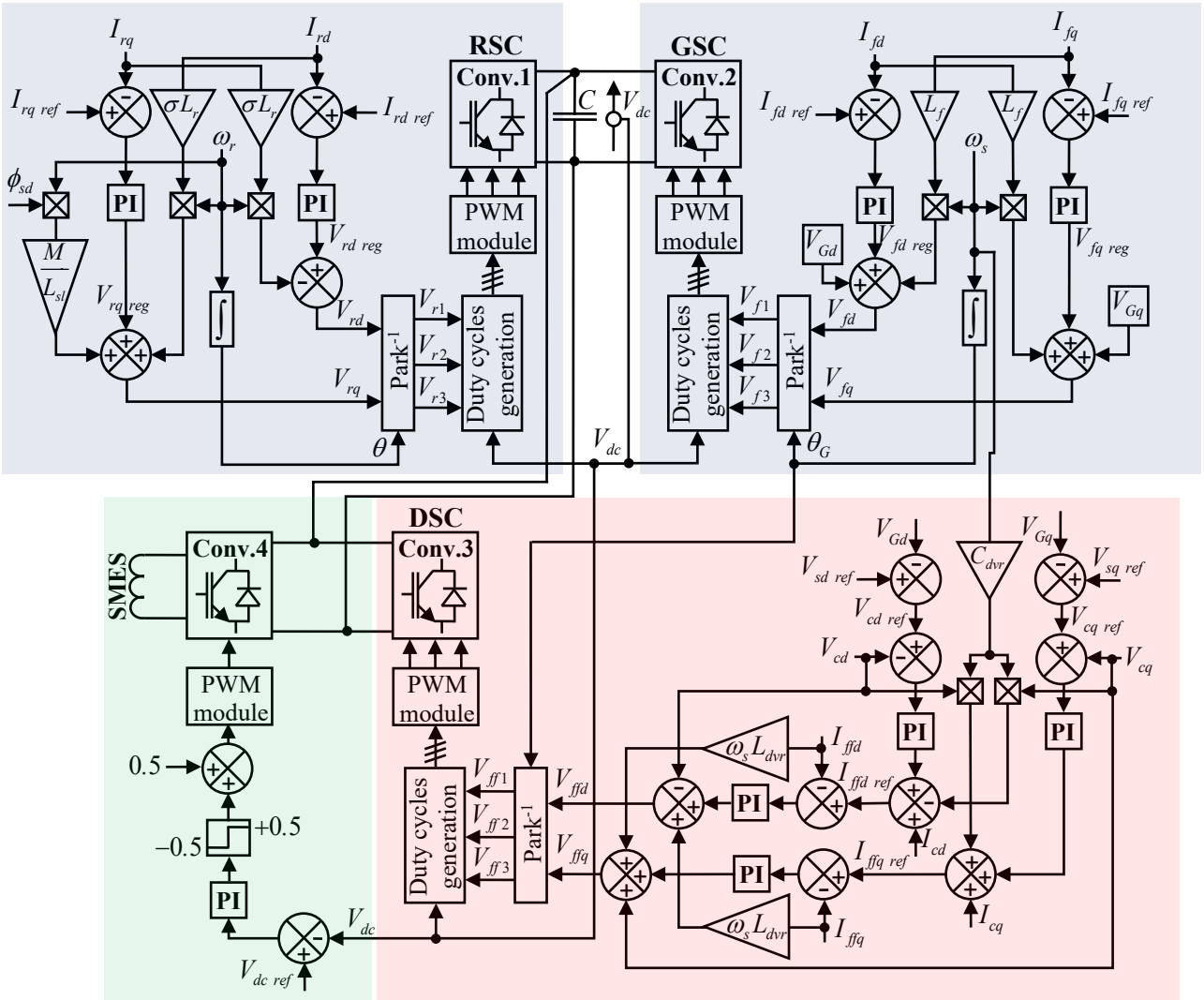

Fig. 2. Control scheme for DFIG_WT with SMES_DVR.

4.1 . DVR modelling and control

The DVR is composed of a voltage source converter DSC connected in series to the system terminals via a perfect transformer and "$L_{dvr}C_{dvr}$" filter. The DVR compensation principle consists in injecting a voltage "V_c" in series with the network voltage "V_G" in case of fault in order to ensure a normal operating condition of the wind turbine [32].

The current and the voltage in the primary and secondary sides of the perfect transformer are given by the following expressions:

$$I_c = -I_g \tag{22}$$

$$V_c = V_s \quad V_{\overline{G}} \tag{23}$$

The "$L_{dvr}C_{dvr}$"filter is connected between the DSC converter and the perfect transformer in order to attenuate the harmonics generated by this converter.

The equations of the filter can be written as follows:

$$V_{ff} = L_{dvr}\frac{dI_{ff}}{dt} \quad V_c \qquad + \tag{24}$$

$$I_{ff} = C_{dvr}\frac{dV_c}{dt} \quad I_c \quad + \tag{25}$$

When transforming Eqs. (24) and (25) in the Park reference frame, we obtain the following equations:

$$V_{ffd} = L_{dvr}\frac{dI_{ffd}}{dt} - \omega_s L_{dvr} I_{ffq} + V_{cd} \tag{26}$$

$$V_{ffq} = L_{dvr}\frac{dI_{ffq}}{dt} + \omega_s L_{dvr} I_{ffd} + V_{cq} \tag{27}$$

$$I_{ffd} = C_{dvr}\frac{dV_{cd}}{dt} - \omega_s C_{dvr} V_{cq} + I_{cd} \tag{28}$$

$$I_{ffq} = C_{dvr}\frac{dV_{cq}}{dt} + \omega_s C_{dvr} V_{cd} + I_{cq} \tag{29}$$

The reference equations of the compensation voltage injected through the perfect transformer in the "$d-q$" axis can be given by:

$$V_{cd\ ref} = V_{sd\ ref} \quad V_{Gd} \quad - \tag{30}$$

$$V_{cq\ ref} = V_{sq\ ref} \quad V_{Gq} \quad - \tag{31}$$

Considering the "PI" controller relationship between various components "$V_{cd,q}$", "$I_{ffd,q}$", the output signal of the DVR command can be expressed according to the following equations:

$$V_{ffd} = PI\left(I_{ffd\ ref} \quad I_{ffd}\right) - \omega_s L_{dvr} I_{ffq} \quad V_{cd} \quad + \tag{32}$$

$$V_{ffq} = PI\left(I_{ffd\ ref} \quad I_{ffd}\right) - \omega_s L_{dvr} I_{ffd} \quad V_{cq} \quad + \tag{33}$$

$$I_{ffd\ ref} = PI\left(V_{cd\ ref} \quad V_{cd}\right) - \omega_s C_{dvr} V_{cq} \quad I_{cd} \quad + \tag{34}$$

$$I_{ffq\ ref} = PI\left(V_{cd\ ref} \quad V_{cd}\right) - \omega_s C_{dvr} V_{cd} \quad I_{cq} \quad + \tag{35}$$

4.2 . SMES modelling and control

SMES has the capability to store energy in the magnetic field created by a direct current flow in a superconducting coil. The SMES is able to absorb or deliver a high power quantity in a short time [33].

The proposed SMES with the bidirectional chopper and the dc link capacitor is presented in Fig. 3.

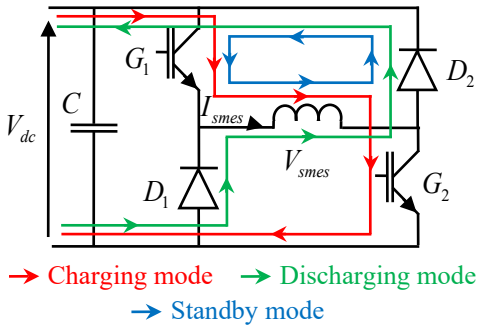

Fig. 3. The DC/DC chopper of the SMES in different operating conditions.

The current exchange direction to or from the SMES depends on the duty cycle of the PWM signals applied to the chopper switches. Initially, the value of the duty cycle is equal to 0.5, the voltage through the SMES is kept constant at zero levels and the current and the energy stored reached a maximum level since there is no energy exchange between the SEMS and the grid.

In case of voltage, the applied value of the duty cycle is less than 0.5. The chopper is activated in discharging mode ("G_1" off and "G_2" off). In this case, the current in the SMES decreases, creating a negative slope "di/dt". Consequently, the voltage through the SMES becomes negative.

In case of a voltage swell, the applied duty cycle is higher than 0.5. The chopper is activated for the charging mode ("G_1" on and "G_2" on). In this case, the current in the coil is increased which creates a positive slope "di/dt". Consequently, the voltages through the SMES become positive. The excess energy is moved to the SMES. The SMES is able to absorb an energy level upper by 30% than the maximum [34].

The mathematical model, which describes the state of the coil in the event of a voltage sag/swell, is given by Eqs. (36) - (41).

The relation between the SMES voltage and the dc-link voltage is given by the following equation [35]:

$$V_{smes} = \left(1 \quad 2D\right)V_{dc} \tag{36}$$

The equation of the coil current depends on voltage "V_{smes}" and the initial current in the SMES "I_{smes_0}" as follows:

$$I_{smes} = I_{smes_0} \quad \frac{1}{L_{smes}} + \int_{t_0}^{t} V_{smes}\, dt \tag{37}$$

The relation between the current across the chopper "I_{chop}" and the current across the SMES coil "I_{smes}" can be expressed as follows:

$$I_{chop} = (1 \quad 2Đ) I_{smes} \tag{38}$$

The power which can be exchanged between the grid and the SMES is given by the following equation:

$$P_{smes} = V_{smes} I_{smes} \tag{39}$$

The energy stored in the SMES is giving by:

$$W_{smes} = W_{smes_0} \int_{t_0}^{t} P_{smes} dt \tag{40}$$

where "W_{smes_0}" represents the initial energy in the SMES and it is expressed as follows :

$$W_{smes_0} = \frac{1}{2} L_{smes} I_{smes_0}^2 \tag{41}$$

5. Simulation Results and Discussion

In order to test the performance of the DFIG_WT based SMES_DVR during the normal operation and the unbalanced voltage conditions, the developed models have been implemented in the MATLAB®/Simulink® software.

The wind speed profile applied to the DFIG WT is variable between "$8ms^{-1}$" and "$14ms^{-1}$" as illustrated in Fig. 4. This choice was based on the WT nominal wind speed which is equal to "$11.5ms^{-1}$" allowing to deliver its nominal power and in order to show the two operation modes "hyper_synchronous and hypo_synhronous" during the total simulation time.

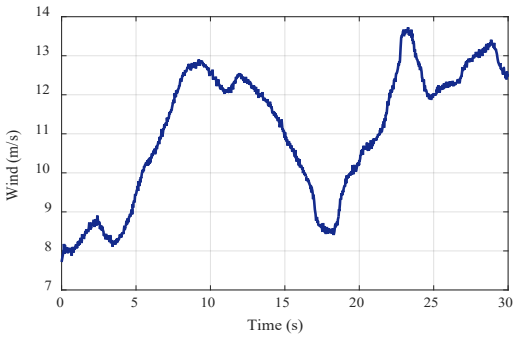

Fig. 4. Wind speed profile.

Fig. 5 and Fig. 6 respectively show the curves of the pitch angle and the power coefficient. According to these two figures, it is observed that if the wind speed exceeds the nominal speed, the pitch angle will be increased in order to limit the WT rotation to its nominal value and ensure a protection from a potential damage. As a result of this variation in the pitch angle, the power coefficient decreases accordingly.

Fig. 7 represents the applied faults at the network voltages. This figure indicates two voltage sags of 20% and 50% and a voltage swell of 20% in order to test the proposed structure in different conditions.

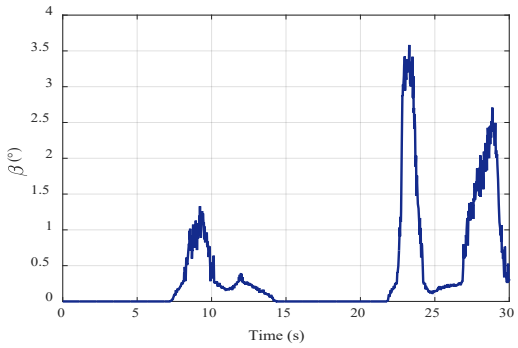

Fig. 5. Pitch angle.

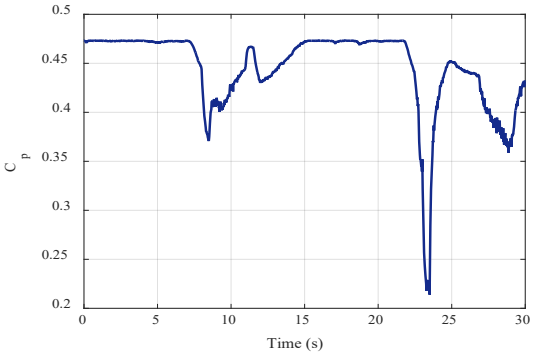

Fig. 6. Power coefficient.

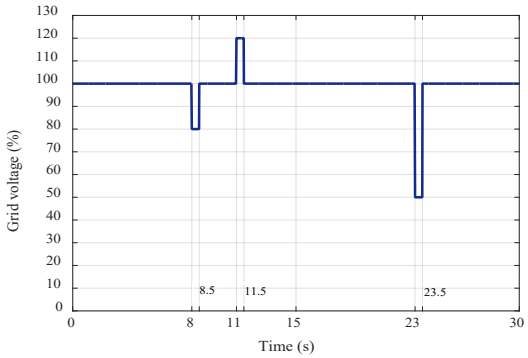

Fig. 7. Grid faults.

In order to put in evidence the developed structure, the DFIG WT was simulated without and with the SMES_DVR system.

Fig. 8 shows that the network voltage unbalance causes directly a variation in the stator voltages. The connection of DVR_SMES to the system has the capability to compensate the stator voltages which return to the normal level in both types of fault. It is observed that in case of LVRT and HVRT, the SMES_DVR device ensures the required energy exchange for the voltage compensation.

Fig. 9 represents the impact of the faults on the WT mechanical speed. In case of a voltage sag, the WT speed increases in order to compensate the active power reduction. In the other case, when a voltage swell occurs, the mechanical speed decreases in order to compensate the active power increases. The applied faults are also justified in the electromagnetic torque variations as shown in Fig. 10. By

installing the SMES_DVR structure, the mechanical speed and the electromagnetic torque are significantly improved.

The active power assessment is presented in Fig. 11. "P_{aero}" is the power available at the wind generator shaft. "P_s" is the stator power supplied to the grid which is limited to the nominal DFIG power. The transfer of the rotor power "P_r" between the grid and the rotor depends on the DFIG operation mode. In hypo-synchronous mode "$\omega_r < \omega_s$" the power "P_r" is extracted from the grid and in hyper-synchronous mode "$\omega_r > \omega_s$", the power "P_r" is injected to the grid. "P_{grid}" is the total power supplied to the grid. It is observed that in case of a voltage swell, the power delivered into the grid will increase to "$1.85MW$" and when a voltage sag occurs at the grid at the time "$t = 23s$", the power injected into the grid will decrease to "$1MW$". However, by the use of the compensation structure, the active power is quickly retained at its normal level.

Fig. 12 shows that the DFIG produces the reactive power to compensate the voltage sag and absorbs the excess of the reactive power in case of a voltage swell. By adding the SMES_DVR structure, the DFIG reactive power delivered is retained to "$0MVAR$" in order to ensure that the power factor remains equal to the unit.

The Fig. 13a illustrates the rotor currents with their references. The rotor current "I_{rd}" is affected by both types of faults since its reference is determined by the stator flux. However, by using the DVR_SMES, the rotor current is decreased to the normal level in a short time as shown in Fig. 13b. The rotor current curve is illustrated in Fig. 14 which indicates the ability of the DFIG to operate in the two modes hyper_synchronous and hypo_synhronous. This curve represents at the time "$t = 6.5s$" the transition from a hypo-synchronous mode to a hyper-synchronous mode and vice versa at the time "$t = 15s$". This figure also represents the effect of the grid voltage faults on the rotor currents. The use of the SMES_DVR in the compensation mode effectively eliminates the influence of both LVRT and HVRT on the rotor current.

Fig. 15 shows that during the grid fault, the amplitude of the filter currents varies according to their references variations. But, when using the proposed structure, these currents are maintained to their normal values.

Fig. 16a shows that the dc-link voltage is regulated to its reference value which is equal to "$1200V$" even in case of grid faults. At the time "$t = 23s$", it is observed that the dc-link voltage represents a peak that reaches "$1400V$". However, by adding the SMES_DVR system, this peak voltage decreases significantly and varies between "$5V$" and "$15V$" according to the zooms of Fig. 16b.

Fig. 17 represents that the "I_c" current in the DC capacitor is oscillating during and after the fault. This oscillation is obtained by the difference found between the currents "I_1" and "I_2". By the use of the SMES_DVR, the DC/DC chopper allows to regulate the current in the dc-link at "$0A$" by the generation or the extraction of the desired current "I_L" to from the SMES. When, the "I_L" current is positive, this indicates that the SMES will deliver energy to the capacitor. Otherwise, when the "I_L" current is negative, this indicates that the SMES is absorbing the excess energy found at the DC bus.

Fig. 18 shows the grid current unstability in both cases of fault. By inserting the SMES_DVR with the DFIG structure, the grid current is improved.

Fig. 19 represents the exchange of energy to/from the SMES during the grid fault. At "$t = 8s$", the energy in the coil will be decreased until "$1.4MJ$" because this energy is delivered to the grid. When the fault is eliminated in "$t = 8.5s$", the coil remains at the level "$1.4MJ$". Therefore, at "$t = 11s$", the energy in the coil will be increased significantly until "$1.55MJ$" as a response to charging the SMES by the excess of energy in the system.

(a) Without compensation

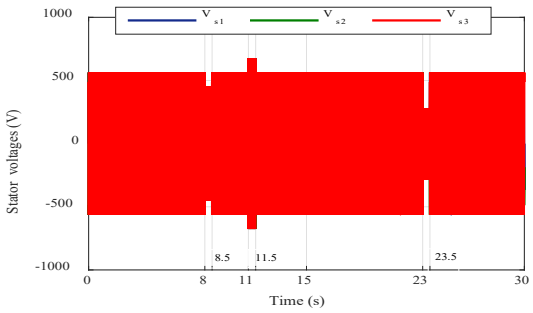

(b) With compensation

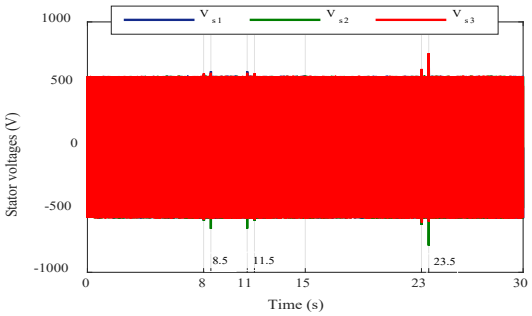

Fig. 8. Stator voltages.

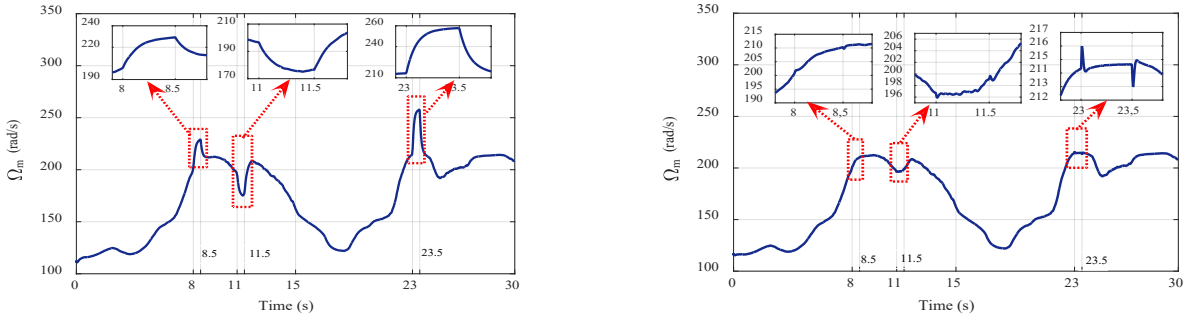

Fig. 9. Mechanical speed.

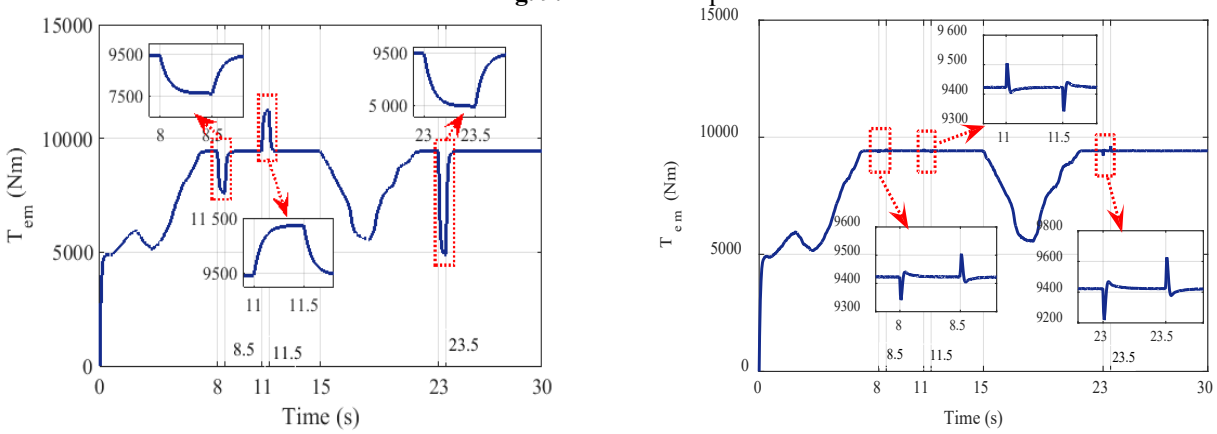

Fig. 10. Electromagnetic torque.

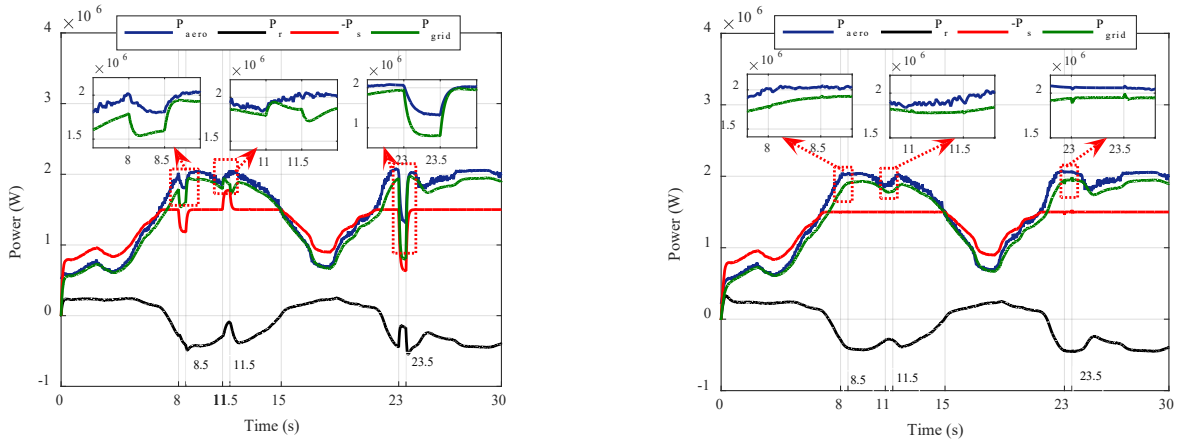

Fig. 11. Active power.

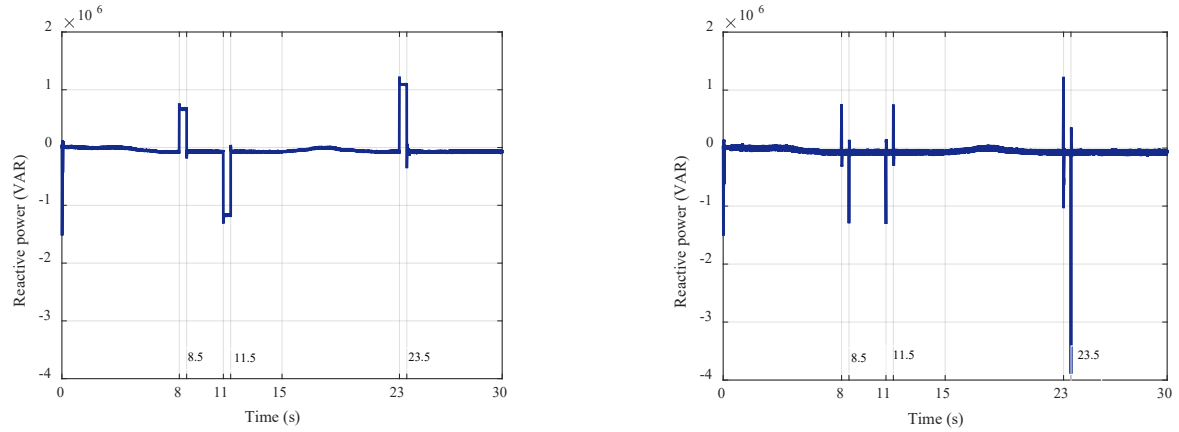

Fig. 12. Reactive power.

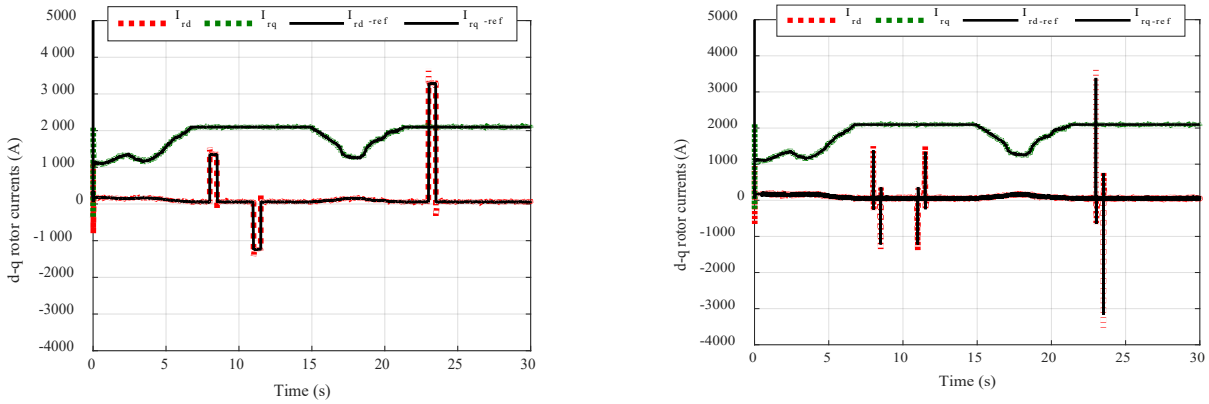

Fig. 13. Rotor current in "$d-q$" farme.

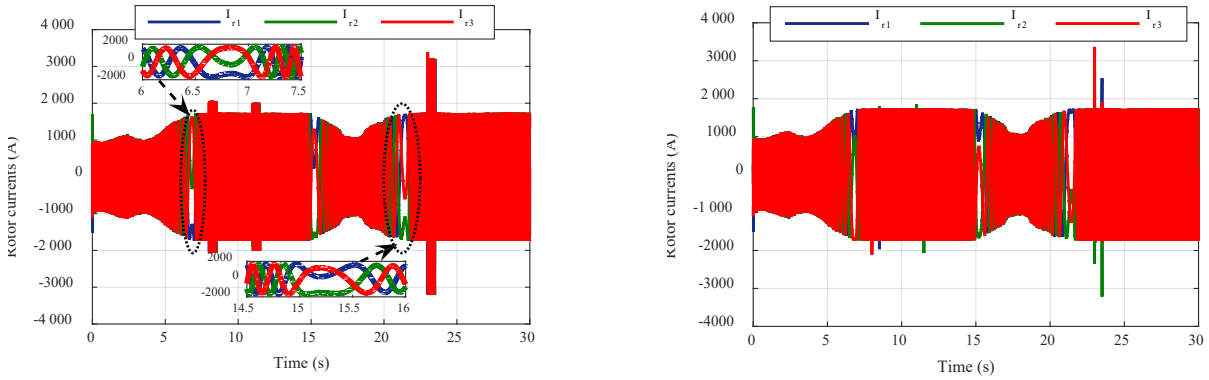

Fig. 14. Rotor currents.

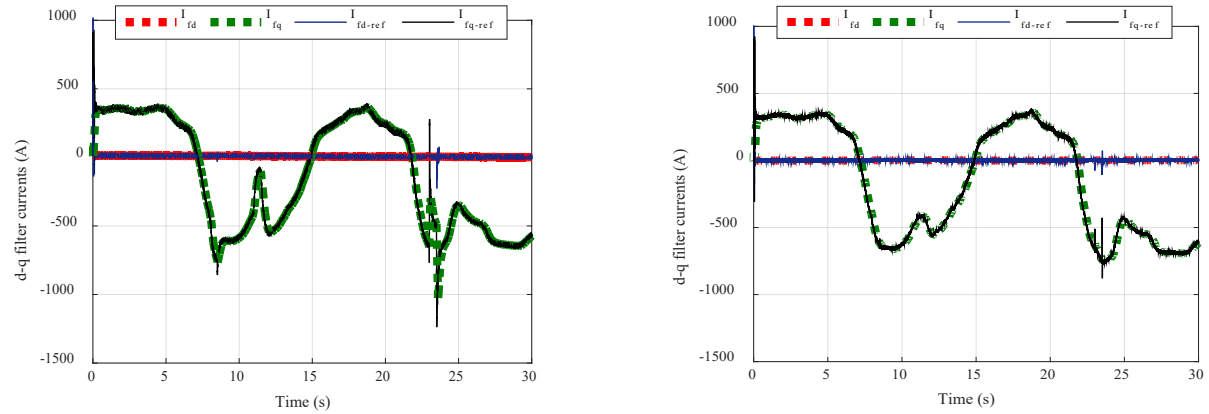

Fig. 15. Filter currents in "$d-q$" farme.

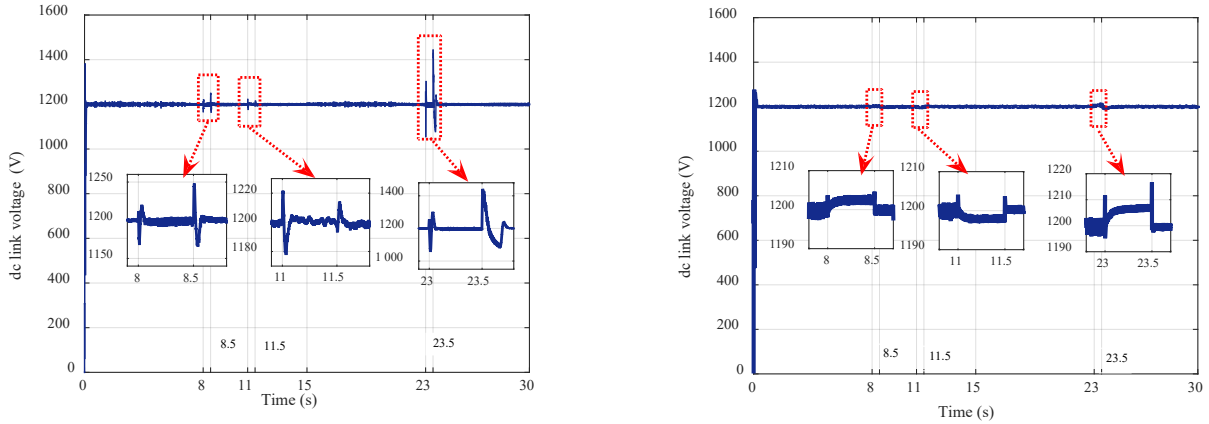

Fig. 16. dc link voltages.

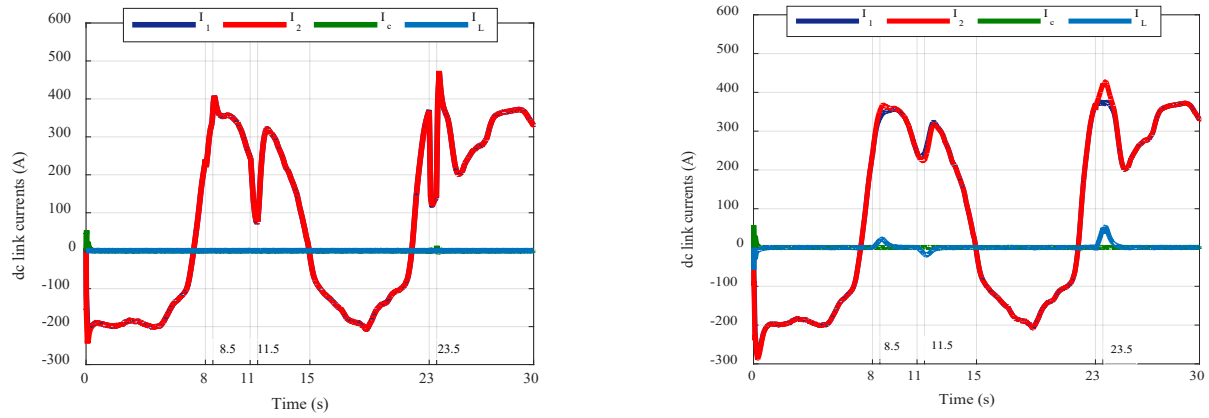

Fig. 17. dc link currents.

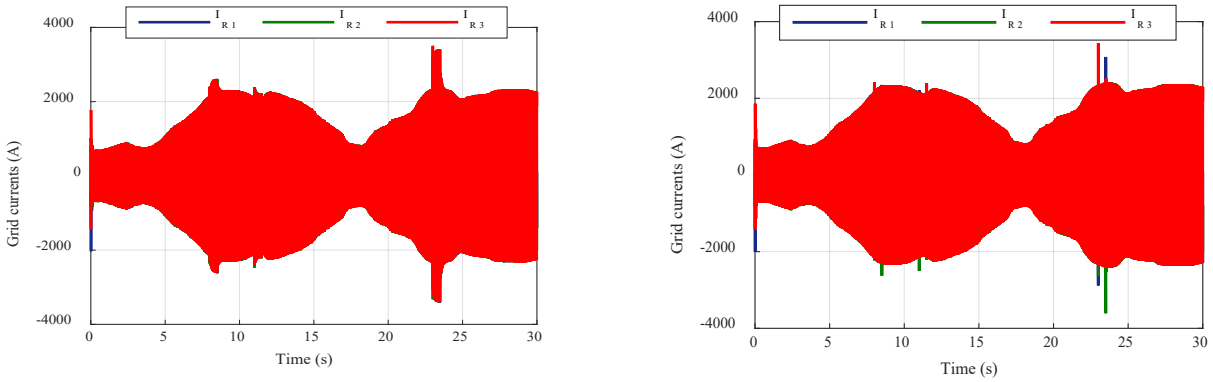

Fig. 18. Grid currents.

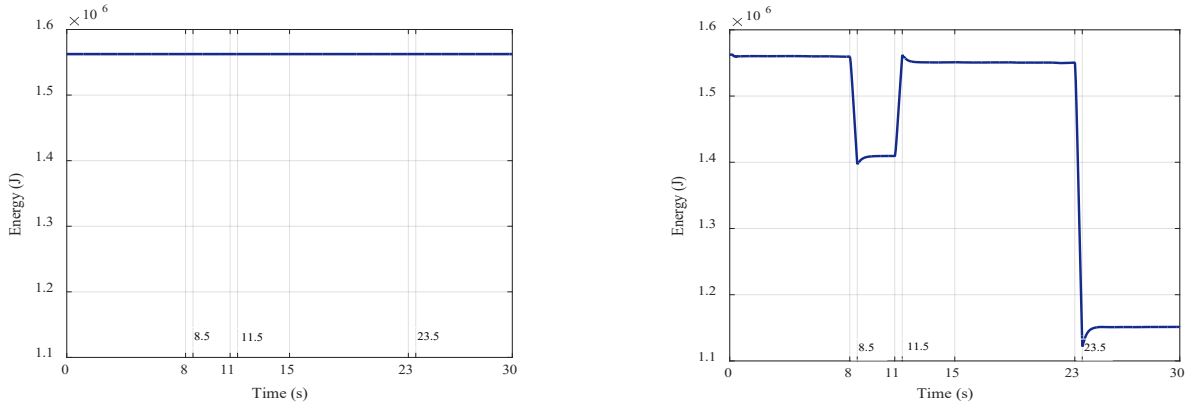

Fig. 19. Energy of the SMES.

6. Conclusion

In this work, a model of DFIG based WT connected to the grid with a suitable controller scheme of a back-to-back converter was developed. Novel equipment SMES_DVR connected with the conventional structure of the DFIG was presented by giving principles and operation modes in order to resolve the problem of LVRT/HVRT. A modified control strategy was used to drive the converters of the new equipments. The designed controllers instantaneously combine between the DVRs active/reactive power control capabilities and SMES energy flow availability. The suggested SMES_DVR component can effectively operates and rapidly react in both LVRT and HVRT by exchanging the required voltage or current with the grid. The simulation results were presented to validate the effectiveness of the proposed strategy in compensating the stator voltage and smoothing the power fluctuations during and after grid faults. In addition, the proposed structure improves the performance of the DFIG for enhancing the FRT capability.

References

[1] Y. E. Abu Eldahab, N. H. Saad, and A. Zekry, "Assessing Wind Energy Conversion Systems Based on Newly Developed Wind Turbine Emulator", International Journal

of Smart Grid, https://doi.org/10.20508/ijsmartgrid.v4i4.133.g101, vol. 4, pp. 139-148, 2020.

[2] A. Petersson, L. Harnefors, and T. Thiringer, "Evaluation of Current Control Methods for Wind Turbines Using Doubly-Fed Induction Machines", IEEE Transactions on Power Electronics, DOI: 10.1109/TPEL.2004.839785, vol. 20, pp. 227-235, 2005.

[3] H. Benbouhenni, "Stator Current and Rotor Flux Ripples Reduction of DTC DFIG Drive Using FSTSMC Algorithm", International Journal of Smart Grid, https://doi.org/10.20508/ijsmartgrid.v3i4.82.g72, vol. 3, pp. 226-234, 2019.

[4] L. Xu, and Y. Wang, "Dynamic Modeling and Control of DFIG-Based Wind Turbines Under Unbalanced Network Conditions", IEEE Transactions on Power Systems, DOI: 10.1109/TPWRS.2006.889113, vol. 22, pp. 314-323, 2007.

[5] Z. Xie, X. Zhang, X. Zhang, S. Yang, and L. Wang, "Improved Ride-Through Control of DFIG During Grid Voltage Swell", DOI: 10.1109/TIE.2014.2370938, IEEE Transactions on Industrial Electronics, vol. 62, pp. 3584-3594, 2015.

[6] A. Safaei, S. H. Hosseinian, and H. A. Abyaneh, "Enhancing the HVRT and LVRT Capabilities of DFIG-based Wind Turbine in an Islanded Microgrid", Engineering, Technology & Applied Science Research, https://doi.org/10.48084/etasr.1541, vol. 7, pp. 2118-2123, 2017.

[7] M. A. S. Ali, K. K. Mehmood, S. Baloch, and C. H. Kim, "Modified rotor-side converter control design for improving the LVRT capability of a DFIG-based WECS", https://doi.org/10.1016/j.epsr.2020.106403, Electric Power Systems Research, vol. 196, pp. 106403, 2020.

[8] F. R. Bada, S. K. Sarker, and S. K. Das, "Transient Stabilization Improvement of Induction Generator Based Power System using Robust Integral Linear Quadratic Gaussian Approach", International Journal of Smart Grid, https://doi.org/10.20508/ijsmartgrid.v3i2.60.g48, vol. 3, pp. 73-83, 2019.

[9] S. Ghosh, Y. J. Isbeih, R. Bhattarai, M. S. El Moursi, E. F. El-Saadany, and S. Kamalasadan, "A Dynamic Coordination Control Architecture for Reactive Power Capability Enhancement of the DFIG-based Wind Power Generation", IEEE Transactions on Power Systems, DOI: 10.1109/TPWRS.2020.2968483, vol. 35, pp. 3051-3064, 2020.

[10] P. H. Huang, M. S. El Moursi, W. Xiao, and J. L. Kirtley Jr, "Novel Fault Ride-Through Configuration and Transient Management Scheme for Doubly Fed Induction Generator", IEEE Transactions on Energy Conversion, DOI: 10.1109/TEC.2012.2222886, vol. 28, pp. 86-94, 2013.

[11] L. Zhou, J. Liu, and S. Zhou, "Improved Demagnetization Control of a Doubly-fed Induction Generator under Balanced Grid Fault", IEEE Transactions on Power Electronics, DOI: 10.1109/TPEL.2014.2382603, vol. 30, pp. 6695-6705, 2015.

[12] V. T. Phan, T. Logenthiran, W. L. Woo, D. Atkinson, and V. Pickert, "Analysis and compensation of voltage unbalance of a DFIG using predictive rotor current control", International Journal of Electrical Power & Energy Systems, https://doi.org/10.1016/j.ijepes.2015.08.020, vol. 75, pp. 8-18, 2016.

[13] J. Liang, D. F. Howard, J. A. Restrepo, and R. G. Harley, "Feed-Forward Transient Compensation Control for DFIG Wind Turbines during both Balanced and Unbalanced Grid Disturbances", IEEE Transactions on Industry Applications, DOI: 10.1109/TIA.2013.2253439, vol. 49, pp. 1452-1463, 2013.

[14] L. Huchel, M. S. El Moursi, and H. H. Zeineldin, "A Parallel Capacitor Control Strategy for Enhanced FRT Capability of DFIG", IEEE Transactions on Sustainable Energy, DOI: 10.1109/TSTE.2014.2371925, vol. 6, pp. 303-312, 2015.

[15] S. B. Naderi, M. Negnevitsky, and K. M. Muttaqi, "A Modified DC Chopper for Limiting the Fault Current and Controlling the DC Link Voltage to Enhance Fault Ride-Through Capability of Doubly-Fed Induction Generator Based Wind Turbine", IEEE Transactions on Industry Applications, DOI: 10.1109/TIA.2018.2877400, vol. 55, pp. 2021-2032, 2019.

[16] A. D. Falehi, and H. Torkaman, "Promoted supercapacitor control scheme based on robust fractional-order super-twisting sliding mode control for dynamic voltage restorer to enhance FRT and PQ capabilities of DFIG-based wind turbine", https://doi.org/10.1016/j.est.2021.102983, Journal of Energy Storage, vol. 42, pp. 102983, 2021.

[17] S. B. Reddy, and M. R. Reddy, "Fuzzy Based Combined Feed-Forward and Feed-Back Controlled Dynamic Voltage Restorer for Enhanced Fault Ride through Capability in DFIG based Wind Turbines", International Journal of Innovative Technology and Exploring Engineering, DOI: 10.35940/ijitee.B7441.129219, vol. 9, pp. 2673-2679, 2019.

[18] A. R. A. Jerin, P. Kaliannan, and U. Subramaniam, "Improved fault ride through capability of DFIG based wind turbines using synchronous reference frame control based dynamic voltage restorer", ISA Transactions, https://doi.org/10.1016/j.isatra.2017.06.029, vol. 70, pp. 465-474, 2017.

[19] A. Moghassemi, and S. Padmanaban, "Dynamic Voltage Restorer (DVR): A Comprehensive Review of Topologies, Power Converters, Control Methods, and Modified Configurations", Energies, https://doi.org/10.3390/en13164152, vol. 13, pp. 4152, 2020.

[20] P. Mukherjee, and V. V. Rao, "Effective location of SMES for power fluctuation mitigation of grid connected doubly fed induction generator", Journal of Energy

Storage, https://doi.org/10.1016/j.est.2020.101369, vol. 29, pp. 101369, 2020.

[21] M. Elshiekh, A. Elwakeel, S. Venuturumilli, H. Alafnan, X. Pei, M. Zhang, and W. Yuan, "Utilising SMES-FCL to improve the transient behaviour of a doubly fed induction generator DC wind system", International Journal of Electrical Power & Energy Systems, https://doi.org/10.1016/j.ijepes.2021.107099, vol. 131, pp. 107099, 2021.

[22] Sonia, and A. K. Dahiya, "Superconducting magnetic energy storage coupled static compensator for stability enhancement of the doubly fed induction generator integrated system", Journal of Energy Storage, https://doi.org/10.1016/j.est.2021.103232, vol. 44, pp. 103232, 2021.

[23] Z. Rafiee, S. S. Najafi, M. Rafiee, M. R. Aghamohammadi, and M. Pourgholi, "Optimized control of Coordinated Series Resistive Limiter and SMES for improving LVRT using TVC in DFIG-base wind farm", Physica C: Superconductivity and its applications, https://doi.org/10.1016/j.physc.2020.1353607, vol. 570, pp. 1353607, 2020.

[24] X. Y. Xiao, R. H. Yang, X. Y. Chen, Z. X. Zheng, and C. S. Li, "Enhancing fault ride-through capability of DFIG with modified SMES-FCL and RSC Control", IET Generation, Transmission & Distribution, DOI: 10.1049/iet-gtd.2016.2136, vol. 12, pp. 258-266, 2018.

[25] L. Chen, G. Li, H. Chen, Y. Tao, X. Tian, X. Liu, Y. Xu, L. Ren, and Y. Tang, "Combined Use of a Resistive SFCL and DC-link Regulation of a SMES for FRT Enhancement of a DFIG Wind Turbine Under Different Faults", IEEE Transactions on Applied Superconductivity, DOI: 10.1109/TASC.2018.2881988, vol. 29, pp. 5600408, 2019.

[26] D. C. Phan, and S. Yamamoto, "Rotor speed control of doubly fed induction generator wind turbines using adaptive maximum power point tracking", Energy, https://doi.org/10.1016/j.energy.2016.05.077, vol. 111, pp. 377-388, 2016.

[27] J. Wang, D. Bo, Q. Miao, Z. Li, X. Wu, and D. Lv, "Maximum power point tracking control for a doubly fed induction generator wind energy conversion system based on multivariable adaptive super-twisting approach", International Journal of Electrical Power & Energy Systems, https://doi.org/10.1016/j.ijepes.2020.106347, vol. 124, pp. 106347, 2021.

[28] E. S. Abdin, and W. Xu, "Control Design and Dynamic Performance Analysis of a Wind Turbine-Induction Generator Unit", IEEE Transactions on Energy Conversion, DOI: 10.1109/60.849122, vol. 15, pp. 91-96, 2000.

[29] F. Mazouz, S. Belkacem, and I. Colak, "DPC- SVM of DFIG Using Fuzzy Second Order Sliding Mode Approach", International Journal of Smart Grid, https://doi.org/10.20508/ijsmartgrid.v5i4.219.g178, vol. 5, pp. 174-182, 2021.

[30] F. Poitiers, T. Bouaouiche, and M. Machmoum, "Advanced control of a doubly-fed induction generator for wind energy conversion", Electric Power Systems Research, https://doi.org/10.1016/j.epsr.2009.01.007, vol. 79, pp. 1085-1096, 2009.

[31] F. Hachicha, and L. Krichen, "Rotor power control in doubly fed induction generator wind turbine under grid faults", Energy, https://doi.org/10.1016/j.energy.2012.05.007, vol. 44, pp. 853-861, 2012.

[32] A. D. Falehi, and M. Rafiee, "Enhancement of DFIG-Wind Turbine's LVRT capability using novel DVR based Odd-nary Cascaded Asymmetric Multi-Level Inverter", Engineering Science and Technology, an International Journal, https://doi.org/10.1016/j.jestch.2017.05.004, vol. 20, pp. 805-824, 2017.

[33] H. S. Salama, and I. Vokony, "Power Stability Enhancement of SCIG and DFIG Based Wind Turbine Using Controlled-SMES", International Journal of Renewable Energy Research, https://doi.org/10.20508/ijrer.v9i1.8817.g7616, vol. 9, pp. 147-156, 2013.

[34] M. G. Rabbani, J. B. X. Devotta, and S. Elangovan, "Application of simultaneous active and reactive power modulation of SMES Unit under unequal a-mode for power system stabilization", IEEE Transactions on Power Systems, DOI: 10.1109/59.761879, vol. 14, pp. 547-552, 1999.

[35] A. M. Shiddiq Yunus, M. A. S. Masoum, and A. Abu-Siada, "Application of SMES to Enhance the Dynamic Performance of DFIG During Voltage Sag and Swell", IEEE Transactions on Applied Superconductivity, DOI: 10.1109/TASC.2012.2191769, vol. 22, pp. 5702009, 2012.